Check for updates

ADVANCED MATERIALS TECHNOLOGIES
www.advmattechnol.de

High Photoluminescence Quantum Yield and Tunable Luminescence Lifetimes in the Sub-Second Range of CaS:Eu^{2+} Phosphors for Tracer Based Sorting

*Arzu Cosgun Ergene, Eduard Madirov, Dmitry Busko, Ian A. Howard, Bryce S. Richards, and Andrey Turshatov**

The shift toward a circular economy for plastics requires innovative sorting technologies that improve recycling efficiency and material purity. Tracer-based sorting (TBS) is a promising approach that employs luminescent tracers with distinct optical properties for the precise identification of plastics. This study presents the synthesis and characterization of europium-doped calcium sulfide (CaS:Eu^{2+}) luminescent materials as potential tracers for TBS. Synthesized via a flux-assisted solid-state reaction, these phosphors achieve photoluminescence quantum yields (PLQYs) of up to 65% with tunable luminescence decay lifetimes ranging from 0.05 to 0.3 seconds. Long-term chemical stability under ambient conditions is confirmed over 18 months. The application of CaS:Eu^{2+} in a TBS prototype is demonstrated using a standard CMOS video camera to differentiate materials based on decay times. These results highlight the suitability of CaS:Eu^{2+} phosphors as stable, high-performance tracers, offering a viable way to improve plastics recycling processes.

1. Introduction

Transitioning to a circular economy for plastics is critical to addressing the global plastic pollution problem. In order to achieve future plastics circularity, it is essential to increase both the quantity and quality of recycled plastic materials for reuse.[1] However, this is a challenging goal with existing recycling technologies, such as mechanical-chemical processes. One of the barriers to high-yield recycling is that spectrometric sorting methods are not powerful enough to differentiate between identical polymer types used in different applications, such as food and non-food grade materials.[2] To overcome this barrier, tracer Bayer AG based sorting (TBS) has recently been introduced to improve near-infrared (NIR) sorting techniques, enabling more comprehensive recycling of plastic waste.[1a,3] In TBS, luminescent materials with unique emission wavelengths can be used in small quantities as tracers to improve sorting.[1c] The most effective approach is to apply the tracers via a printing process or by applying a label containing tracers.[1a] These methods ensure that the optical properties of the tracers remain independent of the polymer matrix. As a result, both the fluorescence spectra and decay characteristics of the tracers are unaffected by the type of polymer used and can be reliably measured.

As previously reported,[1a,b] inorganic luminescent materials (phosphors) serve as tracers based on unique excitation – using X-ray, ultraviolet (UV), visible (vis), or NIR excitation sources – and emission wavelengths and intensities, typically in the vis and NIR range (780–3000 nm in agreement to ISO 20473). In TBS, the sorting of different objects was based on the spectral differences of the tracers. For example, trivalent lanthanide ions exhibit narrow luminescence peaks – for example ytterbium (Yb^{3+}) at ≈1000 nm, holmium (Ho^{3+}) at ≈1200 nm, erbium (Er^{3+}) at ≈1550 nm, and thulium (Tm^{3+}) at ≈1750 nm – that can be resolved using a hyperspectral camera.[1a,b,3,4] However, the number of luminescence peaks is limited and the question arises whether the number of possible tracers can be increased by using a different physical principle.

Although in a static regime, the inherent decay time of autofluorescence of certain polymers has been used as an identification method, without the need for specific tracers,[5] it can be quite challenging to measure the fast (ns or even µs) decay times of an object that is also moving on a conveyor belt at typically 3 m s^{-1}. In contrast, inorganic phosphors offer the advantage of prolonged luminescence decay times, ranging from hundreds of µs to hundreds of ms. Some inorganic phosphors also continue to emit light for extended periods (persistent luminescence), ranging from seconds to hours or even days, after the cessation of the initial excitation source,[6] presenting promising potential for

A. Cosgun Ergene, E. Madirov, D. Busko, I. A. Howard, B. S. Richards, A. Turshatov
Institute of Microstructure Technology
Karlsruhe Institute of Technology
Hermann-von-Helmholtz-Platz 1, 76344 Eggenstein-Leopoldshafen, Germany
E-mail: andrey.turshatov@kit.edu

The ORCID identification number(s) for the author(s) of this article can be found under https://doi.org/10.1002/admt.202500353

© 2025 The Author(s). Advanced Materials Technologies published by Wiley-VCH GmbH. This is an open access article under the terms of the Creative Commons Attribution License, which permits use, distribution and reproduction in any medium, provided the original work is properly cited.

DOI: 10.1002/admt.202500353

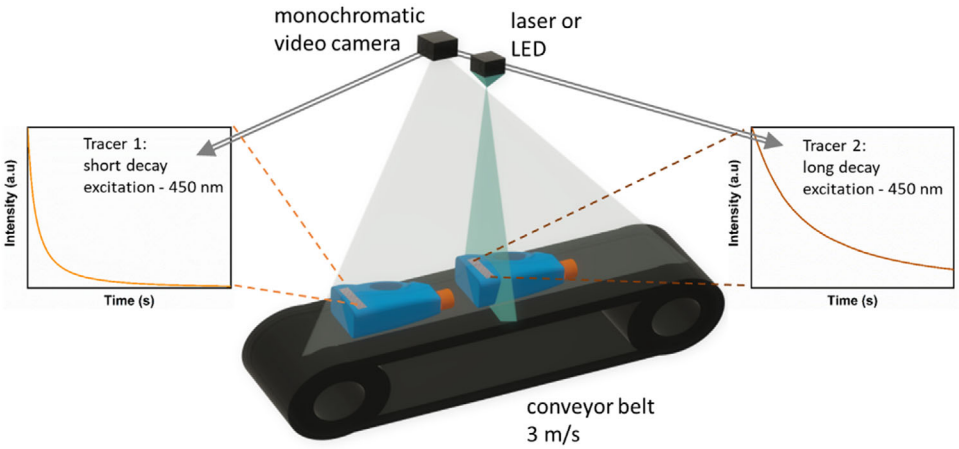

Figure 1. Schematic of a sorting system based on decay time measurements: the labels with two tracers 1 and 2 are printed on the surface of the plastic objects. The tracers have identical excitation and emission spectra but different decay times (short and long) in the sub-second range. The tracers are excited by a 450 nm laser (or LED) with light focused to a line. A monochromatic video camera (with a 450 nm notch filter) records a video which is used to estimate the decay time. Based on the measured decay times, the plastic objects are classified on a conveyor belt (moving at a speed of up to 3 m s^{-1}).

plastic waste sorting applications. However, this approach has yet to be widely explored. Overall, long decay times are beneficial for sorting plastics, as it improve detection reliability. It filters out excitation light and stray fluorescence signals from organic contaminants or additives, which typically decay much faster, on the ns scale.[1c] For example, Becker et al.[7] utilized a combination of organic and inorganic tracers based on emission wavelength and photoluminescence lifetime to identify low-density polyethylene, even when emission wavelengths overlapped. Harris et al.[8] improved waste polymer sorting using inorganic phosphors such as $Y_2O_2S:Eu^{3+}$, whose luminescence can be stimulated by a second infrared light source after charging with UV light.

Thus, it can be attractive to classify different objects according to the luminescence decay time of the tracers, even if all the tracers have similar excitation and emission spectra. If the tracer decay time falls within the range of 0.05–1 second, it can be measured using video recorded with a standard camera, as demonstrated in **Figure 1**. In this figure, the labeled object moves through a line-shaped excitation, and the horizontal displacement corresponding to a decrease in luminescence to 1/e of its initial value represents the luminescence decay time. For decay times of 0.05, 0.15, and 0.3 s, this distance is expected to be 15, 45, and 90 cm (for a conveyor belt moving at a speed of 3 m s^{-1}). By measuring this distance (and the corresponding decay time), different objects can be classified and sorted. This raises two research questions: i) how can a synthetic method be used to tailor the luminescence decay time and to increase the photoluminescence quantum yield (PLQY) of tracers; and ii) how can these tracers be used for plastics sorting. We are therefore looking for luminescent materials with a decay time between 0.05 and 0.3 s, which can be excited with visible light and exhibit bright enough luminescence (with high PLQY) to be measured with a conventional video camera.

In our previous work, we have focused on the decay time of different phosphors in the range of 0.1–10 s for sensing applications using smartphone detection.[9] For example, $CaS:Eu^{2+}$ was synthesized using a solid-state reaction and demonstrated decay times in the range of 0.1–0.6 s with PLQYs in the range of 18–39%.[10] As a further example, the $Gd_2O_2S:Eu^{3+},Ti^{4+}$ samples exhibited longer lifetimes in the range of 1–6 s and also with a good PLQY of ≈46%.[9]

Co-doped alkaline earth metal sulfides, such as MeS (where Me = Be, Mg, Ca, Sr, Ba), are highly effective luminescent materials.[11] These materials serve as suitable hosts for incorporating various dopants and exhibit a wide range of emission wavelengths, covering almost the entire visible spectrum. Divalent europium-doped calcium sulfide ($CaS:Eu^{2+}$) is considered a promising candidate for red phosphors, with potential applications in a wide variety of displays, white light-emitting diodes (LEDs), electroluminescent devices, cell labeling,[12] and medical imaging for solid-state lighting.[13] The strong and broad red emission band of $CaS:Eu^{2+}$ originates from the $5d^1\ 4f^6$ – $4f^7$ transition of Eu^{2+}, with a broad absorption band in the visible wavelength region, making it advantageous for persistent luminescence.[14] The excitation spectrum for this red photoluminescence ranges from 400 to 600 nm, suggesting that $CaS:Eu^{2+}$ could be an effective persistent phosphor for energy storage excited by visible light.[15] With improved PLQY and tunable decay time, these materials can be good candidates for plastic sorting tracers. However, some authors have noted that CaS phosphors may be disadvantageous due to their low chemical stability in the presence of moisture and other atmospheric components, a factor that must be considered.[16]

$CaS:Eu^{2+}$ phosphors have been synthesized by various methods including solvothermal,[17] co-precipitation,[18] solid-state,[19] and microwave-assisted solid-state.[20] Unfortunately, it is difficult to conclude which method produces the best (brightest) phosphor, as the figure-of-merit parameter – PLQY – has not been reported in these papers. Common to all these methods is the need for a reducing atmosphere, which can be provided by elemental sulfur or hydrogen (mixed with nitrogen or argon for safety). On the other hand, another reducing agent – activated carbon – has been actively used to reduce Eu^{3+} to Eu^{2+} in nitride phosphors.[21] An earlier attempt to use carbon in the solid-state

© 2025 The Author(s). Advanced Materials Technologies published by Wiley-VCH GmbH

2365709x, 2025, 19, Downloaded from https://advanced.onlinelibrary.wiley.com/doi/10.1002/admt.202500353 by Karlsruher Institut Für Technologie, Wiley Online Library on [19/11/2025]. See the Terms and Conditions (https://onlinelibrary.wiley.com/terms-and-conditions) on Wiley Online Library for rules of use; OA articles are governed by the applicable Creative Commons License

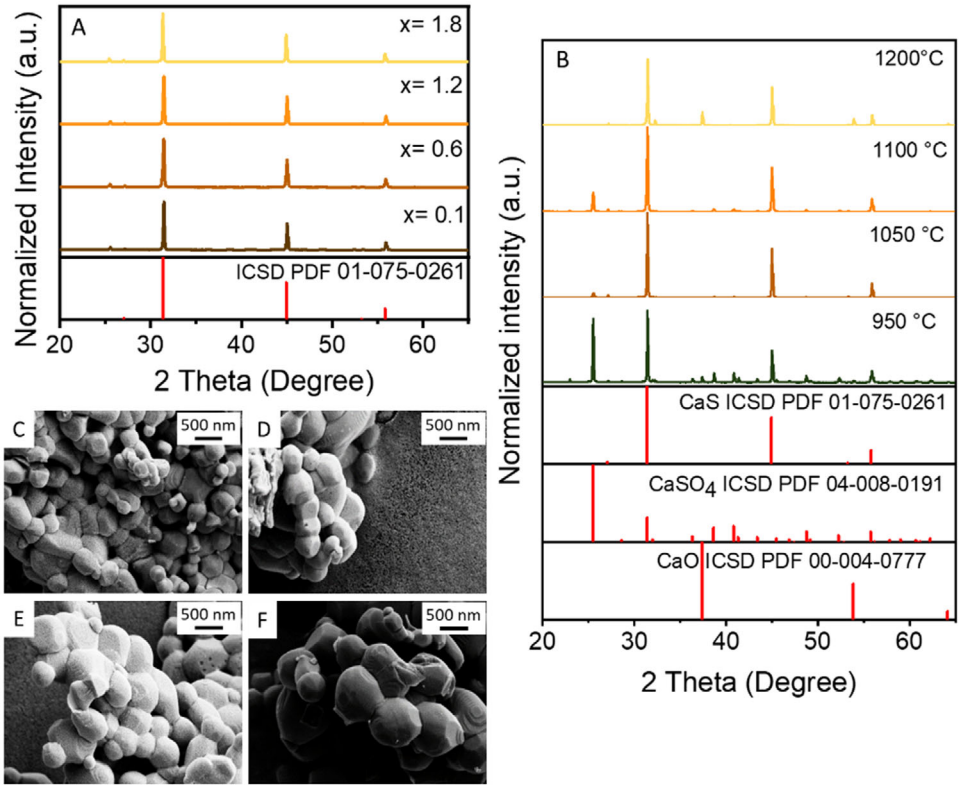

Figure 2. A) XRD patterns of CaS:Eu^{2+} tracers with different Eu^{2+} concentrations; B) XRD patterns of CaS:Eu^{2+} tracers (0.6 mol% Eu^{2+}) synthesized at different temperatures. C–F) SEM image of CaS:Eu^{2+} tracers doped with (C) 0.1 mol% Eu^{2+}, (D) 0.6 mol%Eu^{2+}, (E) 1.2 mol% Eu^{2+} and (F) 1.8 mol% Eu^{2+}.

synthesis of CaS:Eu^{2+} luminophore gave promising results.[22] In our previous work, we combined $CaSO_4$ and Eu_2O_3 precursors with sulfur, activated carbon, and a reduced Ar:H_2 atmosphere to achieve high yields of sulphurization and Eu^{3+} reduction in the solid state reaction. This resulted in PLQY of 39%.[10]

Fluxes are commonly used in the synthesis of inorganic phosphors,[23] including CaS:Eu^{2+}. It has been reported that using a flux (such as Na_2CO_3, Li_2CO_3, NH_4Cl, or NH_4F) can increase the steady-state intensity of the CaS:Eu^{2+} phosphor and improve its moisture resistance.[19b,24] Thus, in the current work, we intend to further increase the PLQY of CaS:Eu^{2+} synthesized by the carbothermal method by applying an additional flux with the aim of increasing the PLQY, chemical resistance, and maintaining the luminescence decay lifetimes of CaS:Eu^{2+} in the sub-second range. We deliberately chose the NH_4Cl flux, which provided the second most intense luminescence (after NH_4F) in the work by Guo et al.[19b] because this flux doesn't generate toxic hydrofluoric acid during the synthesis. Four CaS:Eu^{2+} samples with different Eu^{2+} concentrations were used to demonstrate the feasibility of detecting decay times using a conventional video camera, thus opening up new possibilities for TBS based on decay time detection.

2. Results and Discussion

The X-ray diffraction (XRD) patterns of Eu^{2+} doped CaS samples are shown in **Figure** 2A,B. The XRD patterns of various amounts of Eu^{2+}-doped CaS exhibit well-defined diffraction peaks that match the standard pattern of CaS, PDF 01-075-0261, and a cubic lattice structure with the Fm-3m space group. In order to optimize the flux-assisted synthesis we investigated the effect of temperature on the properties of CaS tracers with 0.6 mol.% Eu^{2+}. Figure 2B presents the XRD analysis of samples synthesized at 950 °C, 1050 °C, 1100 °C, and 1200 °C. The results indicate the presence of $CaSO_4$ at 900 °C and CaO at higher temperatures (1100 °C and 1200 °C). Only the reaction at 1050 °C yields a pure CaS phase without impurities. Therefore, this temperature was selected to vary the Eu^{2+} content in the samples. In this experiment, CaS samples with four concentrations of Eu^{2+} (0.1, 0.6, 1.2, and 1.8 mol%) demonstrate similar diffraction peaks as presented in Figure 2A.

The morphology of Eu^{2+}-doped CaS samples was characterized using a scanning electron microscope (SEM). Agglomerated particles within the micron size range were observed. The morphology of the samples showed no significant changes with the addition of Eu^{2+} ions (Figure 2C–F; Figure S1, Supporting Information).

The synthesized sample demonstrates a strong peak (472 nm) in PLE spectra (**Figure** 3A). This peak in the visible range is associated with the $4f^7 \rightarrow 4f^65d^1$ transition of Eu^{2+}. The additional peak observed in the excitation spectrum at 248 nm corresponds to the energy bandgap transition of CaS. Excitation using LED (450 nm) leads to strong luminescence with the emission peak at 654 nm (similar to all samples). This broadband red emission

© 2025 The Author(s). Advanced Materials Technologies published by Wiley-VCH GmbH

2365709x, 2025, 19, Downloaded from https://advanced.onlinelibrary.wiley.com/doi/10.1002/admt.202500353 by Karlsruher Institut Für Technologie, Wiley Online Library on [19/11/2025]. See the Terms and Conditions (https://onlinelibrary.wiley.com/terms-and-conditions) on Wiley Online Library for rules of use; OA articles are governed by the applicable Creative Commons License

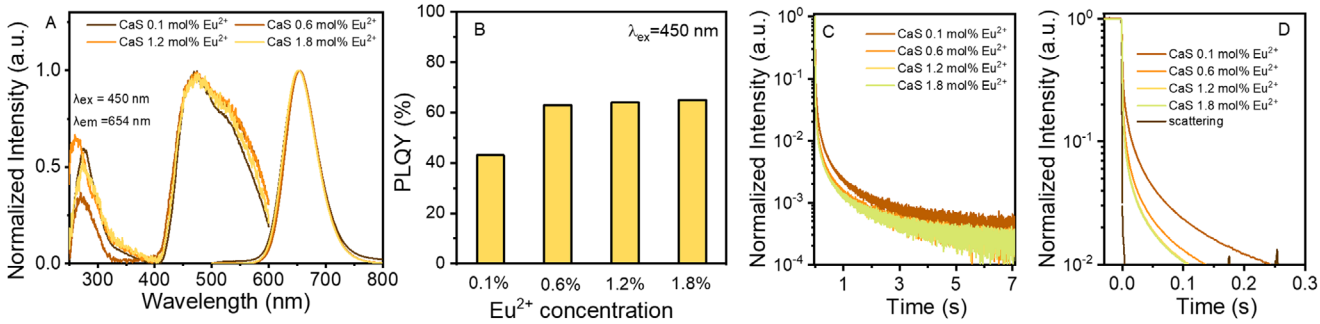

Figure 3. A) Normalized PL and PLE spectra of CaS:Eu^{2+} tracers, B) PLQY value of CaS:Eu^{2+} tracers measured in an integrating sphere; C) PL decays of CaS:Eu^{2+} tracers; D) PL decays of CaS:Eu^{2+} tracers during the first 0.3 s.

results from an electric dipole-allowed interconfigurational transition between the $4f^6 5d^1$ excited state and the $4f^7$ ground state.[25]

The figure-of-merit parameter of luminescence materials is the absolute PLQY defined as a ratio between the number of emitted photons to the number of absorbed photons, and was measured using an integrating sphere. The PLQY measurements were performed for two batches of CaS:Eu^{2+} and the deviations did not exceed three relative percentages, which is the expected uncertainty value for the PLQY measurements reported in our previous publication.[26] For example, a maximum PLQY value of 65 ± 2% was measured for the "CaS 0.6 mol% Eu^{2+}" sample. For simplicity, the uncertainties of the PLQY measurements are omitted from the further discussion. Figure 3B shows that three samples with 0.6, 1.2, and 1.8 mol.% Eu^{2+} demonstrates similar PLQY in the range of 63–65%. These high values indicate a minimal level of concentration quenching within this concentration range. This is consistent with earlier published results for $Ba_{2-x}LiB_5O_{10}$:xEu^{2+},[27] $Li_2Ba_{1-x}Eu_xSiO_4$:xEu^{2+}[28] and $Ca_{2-x}BO_3Cl$:xEu^{2+}[29] where critical quenching concentrations of x = 0.03, 0.01 and 0.03, respectively, were observed.

It should be noted that the measured PLQY values are as high as 65%, which is the value measured for a single crystal of a standard green persistent phosphor such as $SrAl_2O_4$:Eu^{2+},Dy^{3+}[30] and often exceed the previously reported PLQY values for deep red persistent phosphors, such as $Ca_{14}Mg_4Ga_{12}O_{36}$:Mn^{4+} (51%),[31] $ZnGa_2O_4$:Cr^{3+} (31%,[32] 48%[33] and 98.6%[34]) and CaS:Eu^{2+} (39%).[10]

In addition, Figure S2 (Supporting Information) shows the PLQYs of CaS samples with 0.6% Eu^{2+} synthesized at different temperatures. The PLQYs are significantly lower (in the range 21–36%) when the samples are synthesized at temperatures other than the optimal 1050 °C. These results are consistent with the XRD analysis, which shows the absence of a pure CaS phase at synthesis temperatures of 950 °C, 1100 °C, and 1200 °C.

Significantly, we evaluated the PLQY of powder samples containing 0.1% and 0.6% Eu^{2+} after prolonged storage of 18 months under ambient conditions. The samples were stored in closed (but not sealed) polymethyl methacrylate containers at 23 ± 5 °C and 40 ± 10% relative humidity. Notably, the PLQY remained unchanged after 18 months, retaining values of 44% and 65% for 0.1% and 0.6% Eu^{2+}, respectively. This finding motivated us to perform the stability test under challenging conditions and to compare the stability of the CaS:Eu^{2+} phosphor with the benchmark phosphor – commercial $SrAl_2O_4$:Eu^{2+},Dy^{3+}. The materials were tested under conditions corresponding to the accelerated life test: 85 °C and 85% RH ("double 85" or "damp-heat" test), typically applied in the photovoltaic field.[35] We compared the stability of two representative situations – raw materials (as powder) and raw materials incorporated into a lacquer layer, based on commercial thermostable white lacquer. In general, there is not yet a common standard for testing phosphors for plastic sorting applications. However, we believe that the "damp-heat" test is one of the harshest environmental tests. This is indeed why we chose it.

XRD analysis of the raw powders after the "damp-heat" test shows that both commercial phosphors, $SrAl_2O_4$:Eu^{2+},Dy^{3+}, and CaS:Eu^{2+}, degrade significantly even after 1 h under conditions of elevated temperature and humidity (**Figure** 4A,B). However, a small quantity of the original phases, $SrAl_2O_4$ and CaS, can be found after 17 h of the "damp-heat" test. For the phosphors embedded in the lacquer layer, we tested the intensity of the luminescent peak as a function of test time (Figure 4C). The luminescence intensity decreased by 40% for the CaS:Eu^{2+} phosphors and by 58% for the $SrAl_2O_4$:Eu^{2+},Dy^{3+} phosphors after 1 h of testing. CaS:Eu^{2+} luminescence retains 32% of its pre-test intensity, whereas $SrAl_2O_4$:Eu^{2+},Dy^{3+} luminescence completely vanishes after 72 h of the "damp-heat" test. These results suggest that the CaS:Eu^{2+} tracers are more chemically stable than the benchmark $SrAl_2O_4$:Eu^{2+},Dy^{3+} phosphor over the tested periods.

In agreement with the proposed concept (Figure 1), it is desirable to have tracers with decay times in the sub-second range. Figure 3C shows the decays of the samples with different doping concentrations of Eu^{2+}. The CaS:Eu^{2+} samples exhibit persistent luminescence, emitting for several seconds after an excitation pulse. All decay profiles are polyexponential and cannot be accurately fitted, even with a three-exponential model. All decays exhibit a fast decay component with a decay time of less than 100 µs, corresponding to the intrinsic luminescence of Eu^{2+} (Figure 3D). Longer decay times (on ms and s time scale) are attributed to the involvement of various trap states in the Eu^{2+} luminescence.

To better understand the properties of the trap, we performed TL analysis on the samples (**Figure** 5). All samples demonstrate a maximum of luminescence at 218 K. This peak corresponds to shallow traps with an activation energy of 0.26–0.28 eV (see Figure S3 and Table S1, Supporting Information). These shallow traps are assumed to be responsible for the fast sub-second lifetimes observed in Figure 3C,D. An increase in the concentration of Eu^{2+} (0.6 mol% and higher) results in the appearance of a

© 2025 The Author(s). Advanced Materials Technologies published by Wiley-VCH GmbH

2365709x, 2025, 19, Downloaded from https://advanced.onlinelibrary.wiley.com/doi/10.1002/admt.202500353 by Karlsruher Institut Für Technologie, Wiley Online Library on [19/11/2025]. See the Terms and Conditions (https://onlinelibrary.wiley.com/terms-and-conditions) on Wiley Online Library for rules of use; OA articles are governed by the applicable Creative Commons License

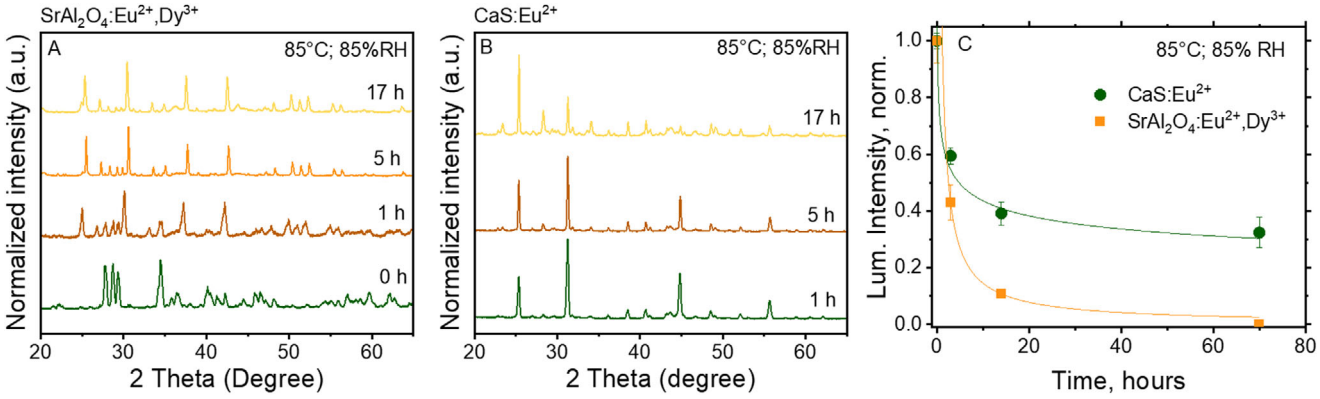

Figure 4. A) XRD patterns of $SrAl_2O_4:Eu^{2+},Dy^{3+}$ powder measured after 1, 5, and 17 h in a climate chamber at 85 °C and 85% RH; B) XRD patterns of CaS 0.6 mol% Eu^{2+} powder, measured after 1, 5, and 17 h in a climate chamber at 85 °C and 85% RH; and C) the luminescence of lacquer layers with $SrAl_2O_4:Eu^{2+},Dy^{3+}$, and CaS 0.6 mol% Eu^{2+} as a function of time in a climate chamber at 85 °C and 85% RH.

second peak in the TL curve with a temperature maximum at 320 K for all three samples. Thus, a new population of traps with a higher activation energy of 0.42–0.44 eV is formed (Figure S3 and Table S1, Supporting Information). While there is no absolute proof, the appearance of these new traps may be responsible for the decrease in sub-second lifetime (Figure 3C,D), as energy may migrate from the shallow traps (with an energy of 0.26–0.28 eV) to these newly formed deeper traps.

For practical use, we have defined the characteristic decay time (τ_{cdt}) as the time at which intensity drops from $I_1 = 10^{-1} \times I_0$ to $I_2 = 10^{-1} \times I_1$. The characteristic intensity I_1 was chosen on the assumption that in further experiments a CMOS camera would not be able to resolve the µs lifetime responsible for the rapid decrease in intensity from the I_0 value, while the sensitivity of the CMOS camera and the signal-to-background signal would not be able to quantify values below I_2. These values do not carry any important scientific information but are necessary to identify different tracers. The longest τ_{cdt} of 0.215 s was measured for the sample with 0.1 mol% Eu^{2+}. An increase in doping concentration leads to τ_{cdt} of 0.129 s and 0.102 s for samples with 0.6 mol.% and 1.2 mol.% Eu^{2+}, respectively. The apparent decay time doesn't change with the next increase in concentration and is 0.102 s for the sample with 1.8 mol% Eu^{2+}. Thus, a question arises: can the difference in τ_{cdt} values be detected using a CMOS video camera, and do the samples with 1.2 mol% and 1.8 mol% Eu^{2+} appear identical when measured using the camera?

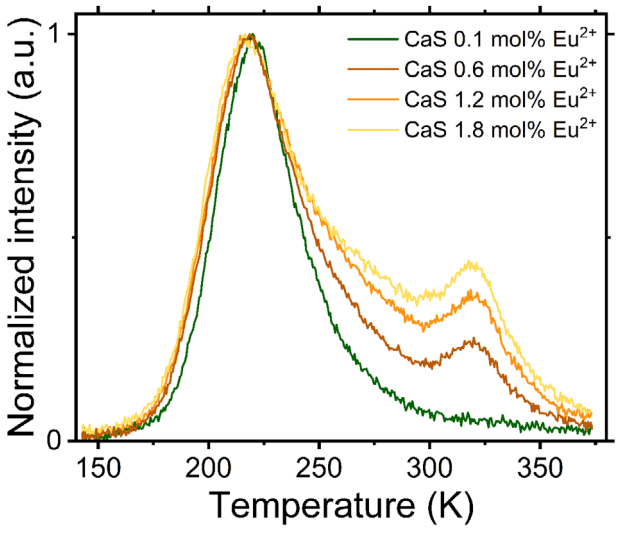

Figure 5. Normalized thermoluminescence curves of $CaS:Eu^{2+}$ samples. The samples were charged using 450 LED (5 min) and measured after 5 min fading time.

To prove that the decay of a moving object labeled with $CaS:Eu^{2+}$ tracer can be measured in the I_1–I_2 range with a CMOS video camera, we performed the following experiment. As it is difficult to construct a conveyor belt moving at 3 m s^{-1} in an optical laboratory, we placed the tracers on a disc rotating at a frequency of 10 Hz. The tracers passed through the excitation spot and moved further at a speed corresponding to a linear velocity in the range of 2.8–4.1 m s^{-1} (the velocity depends on the position of the tracer relative to the disk center). The luminescence of the tracers was recorded with a CMOS camera. On rotation, the tracers produce a characteristic trajectory (**Figure** 6A). A Python code – detailed in the supplementary information (SI) – allows us to linearize the trajectory (Figure 6B and extract decay curves (Figure 6C). It is assumed that the beginning of the decays in Figure 3C corresponds to intensity I_1. Thus, the τ_{cdt} (time for the decay drop from t_1 to $t_2 = 10^{-1} \times t_1$) was calculated as 0.081, 0.056, 0.059, and 0.070 s for tracers with 0.1, 0.6, 1.2, and 1.8% Eu^{2+}, respectively. The τ_{cdt} values measured using a CMOS camera and rotating disk are expected to differ from results obtained using the spectrometer. This discrepancy can be attributed to the undefined zero time in the experiment involving the rotating disk, where the large excitation spot overlaps with the onset of the luminescence decay. However, the decays shown in Figure 4C follow a similar trend to those in Figure 3C. The longest τ_{cdt} corresponds to the tracer with 0.1% Eu^{2+}, while the shortest τ_{cdt} is observed for the tracers with 0.6 and 1.2% Eu^{2+}. The outlier behavior of τ_{cdt} for the tracer with 1.8% Eu^{2+} can be attributed to the weakest luminescence intensity (amplitude at zero time) observed for this tracer. This intensity is at least two times weaker than for other decays due to the non-equal intensity distribution within the excitation spot produced by the LED source. In order to assess the experimental errors, a worst-case scenario is considered when two tracers are excited with different intensities. For

© 2025 The Author(s). Advanced Materials Technologies published by Wiley-VCH GmbH

2365709x, 2025, 19, Downloaded from https://advanced.onlinelibrary.wiley.com/doi/10.1002/admt.202500353 by Karlsruher Institut Für Technologie, Wiley Online Library on [19/11/2025]. See the Terms and Conditions (https://onlinelibrary.wiley.com/terms-and-conditions) on Wiley Online Library for rules of use; OA articles are governed by the applicable Creative Commons License

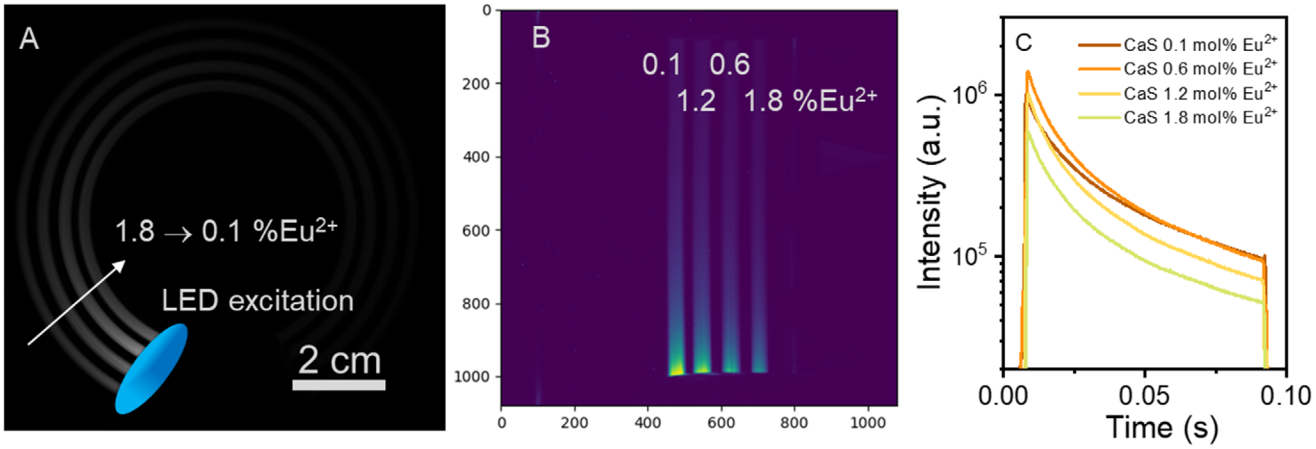

Figure 6. A) photo of a disk with printed tracer spots that rotate at 10 Hz. The tracers are periodically excited with LED source (450 nm). B) linearized trajectories from (A); C) luminescence decays obtained from Figure 4B.

this scenario, we should note the relative difference in the rotating disc experiment for tracers with 1.2 and 1.8% of Eu^{2+}.

This difference is (0.071 s – 0.056 s)/0.071 s = 0.156. However, from the precise experiment in Figure 3C it is known that τ_{cdt} tracers with 1.2 and 1.8% of Eu^{2+} should be equal. Therefore, we can deduce the relative error in the rotating disc experiment to be 15.6%.

In the approach illustrated in Figure 1, the video camera records a video of the moving object, rather than a single image, to estimate the decay time. For instance, this method enables the system to measure the lateral displacement of tracers (and corresponding objects) using the video footage. The displacement is determined between the point of tracer excitation (I_1) and the point where the luminescence intensity decreases to $t_2 = 10^{-1} \times t_1$. As this displacement is proportional to the decay time, it serves as a basis for classifying the sorted objects – for τ_{cdt} values of 0.081 and 0.057 s we can expect the displacement (at a conveyor belt speed of 3 m s^{-1}) of 24.1 ± 3.7 cm and 17.1 ± 2.7 cm (where the absolute errors were estimated using the relative error of 15.6% discussed previously). It is expected that this difference in displacement can be reliably measured for two tracers with 0.1 and 0.6 (or 1.2 or 1.8) % Eu^{2+}. The accuracy of the measurement can be improved by realizing a homogeneous (in terms of intensity) linear irradiation of a conveyor belt using the LED of a laser source. With these improved conditions, more than two tracers could be resolved in combination with the extended range of the available τ_{cdt}, which also requires further synthesis effort.

3. Conclusion

In conclusion, the europium-doped calcium sulfide ($CaS:Eu^{2+}$) phosphors synthesized by a flux-assisted solid-state reaction exhibit promising properties for TBS applications. The high PLQY (up to 65%) and tunable luminescence decay times in the sub-second range provide a practical basis for their use in plastic waste sorting. The demonstrated stability of these phosphors under ambient storage conditions for 18 months further reinforces their suitability for real-world applications. Experimental validation using a CMOS camera confirms the feasibility of discriminating decay times for efficient plastic sorting. These results suggest that the newly developed $CaS:Eu^{2+}$ phosphors offer a useful addition to established sorting techniques, such as NIR sorting and TBS based on measurements of luminescent spectra, providing a way to enhance the accuracy and consistency of recycling processes and supporting efforts toward improved plastics circularity.

4. Experimental Section

Materials: $CaS:Eu^{2+}$ phosphors were prepared by a solid-state reaction method from $CaSO_4$ (purity, < 99%, VWR—Alfa Aesar), Eu_2O_3 (purity, 99.99%, Sigma–Aldrich), sulfur (ChemPur, purity 99+ %), activated carbon (ChemPur, powder < 100 µm), and NH_4Cl (ChemPur, purity 99+ %) as flux without further purification.

Synthesis: A series of $Ca_{1-x}S:Eu_x^{2+}$ ($0.001 < x < 0.018$) phosphors were synthesized using a solid-state synthesis technique. The precursors were mixed with pure ethanol and 4 wt.% NH_4Cl and ground in an agate mortar and pestle for ≈20 min. Activated carbon was introduced to improve the reduction efficiency. The resulting mixture was then allowed to dry, transferred to a crucible, and annealed at different temperatures (in the range 950–1200°C) for 1 h in a reductive atmosphere ($Ar:H_2 = 95:5$) using a heating ramp rate of 10°C min^{-1} in a tube furnace (MTI Corporation, GSL1500X). The samples were then cooled to room temperature, and the finely ground powder was used for all subsequent measurements.

Characterization: Crystal structure analysis and phase identification were performed by X-ray powder diffractometer (Bruker, D2 Phaser) equipped with Cu Kα radiation (1.5405 Å), scanning rate 1 s per step, 0.02° increment, over a 2θ range of 20°–70°).

The synthesized powders' microstructure was imaged using a scanning electron microscope (SEM, Zeiss, SUPRA 60VP) equipped with an SE-II detector. The samples were sputter-coated with 10 nm of silver to enhance SEM imaging.

Stability Test: In the first set of experiments, a representative CaS 0.6 mol%Eu^{2+} sample and a reference phosphor (commercial $SrAl_2O_4:Eu^{2+}$, Dy^{3+}, Aldrich) were placed in a climatic chamber (DM340-CS-R, ACS) at a temperature of 85 °C and a relative humidity of 85% RH. Samples were removed from the chamber after 1, 5, and 17 h, dried at 150 °C for 1 h in a Phoenix BLACK microwave furnace (CEM Corporation), and characterized by XRD. In the second set of experiments, $CaS:Eu^{2+}$ and $SrAl_2O_4:Eu^{2+},Dy^{3+}$ powders were mixed (5 wt.%) with a commercial lacquer (Schöner Wohnen). The lacquer layers were cast onto glass microscope slides using the doctor blade method and left to dry overnight at room temperature, resulting in solid white films with a thickness of ~200 µm. These films were then placed in the climate chamber

© 2025 The Author(s). Advanced Materials Technologies published by Wiley-VCH GmbH

2365709x, 2025, 19, Downloaded from https://advanced.onlinelibrary.wiley.com/doi/10.1002/admt.202500353 by Karlsruher Institut Für Technologie, Wiley Online Library on [19/11/2025]. See the Terms and Conditions (https://onlinelibrary.wiley.com/terms-and-conditions) on Wiley Online Library for rules of use; OA articles are governed by the applicable Creative Commons License

(DM340-CS-R, ACS). Luminescence spectra from the same spot on the film were measured using a spectrofluorometer (Edinburgh Instruments, FS5) after 3, 14, and 72 h in the climate chamber. To demonstrate the repeatability of the luminescence measurements, the film was measured five times, with the film removed from the spectrofluorometer and replaced each time. Due to the very long decay time of the $SrAl_2O_4:Eu^{2+},Dy^{3+}$ sample, it was irradiated with a white LED for 5 min before the luminescence spectra were measured (to reach steady state luminescence intensity).

Optical Methods: The PLQY was measured with a custom-built optical setup built around an integrating sphere. The sample was placed in an integrating sphere (Labsphere, 6 in. Ø, 3 P-LPM-060-SL) and excited with a continuous-wave diode operating at 450 nm (Thorlabs, M450LP1) and driven by a LED diode driver (Thorlabs, LEDD1B). The emission was collected with a spectrometer (Avantes, AvaSpec-ULS2048×64TEC-EVO) via the collecting fiber (Thorlabs, BFY200MS02).

The excitation and emission spectra were collected with a spectrofluorometer (Edinburgh Instruments, FS5) equipped with a Xe lamp as an excitation source and a PMT as a detector.

Lifetime measurements were performed using a LED (Thorlabs, M450LP1), pulsed using a driver (Thorlabs, ITC4001), and a Si-detector (Thorlabs, PDA100A). The scattered LED radiation was rejected with a long-pass filter (FELH0550, Thorlabs). The acquisition and digitalization were done using a DAQ card (NI USB-6251), with a self-written procedure automated in LabVIEW. For a noise reduction, decay profiles were averaged over 100 pulses.

The thermoluminescence (TL) data were obtained using a home-built setup assembled around a heating stage (Microptik BV, MTDC600), which operates within a temperature range of 83–875 K. In a typical experiment, a sample was irradiated (charged) for 5 min using a 450 nm LED (Thorlabs, M450LP1) with an intensity of ≈100 mW cm^{-2}. After a 5-min fade time, the sample was heated at a rate of 0.5 K/s and its luminescence was measured using an Avantes AvaSpec-ULS2048×64TEC-EVO fibre-coupled spectrometer. The thermoluminescence glow curve was deconvoluted using the glow curve deconvolution (GCD) method (see Supporting Information) similar to previous publications.[36,37]

A demonstration experiment with a spinning disk was done using a black PMMA sheet mounted on a chopper. The rotation speed of was chosen of 10 Hz. The sample's material was mixed with transparent nail polish and applied as dots on a PMMA-sheet surface. The excitation LED (Thorlabs, M450LP1) was mounted in front of the spinning disc to irradiate a circle ≈25 mm in diameter. The LED light was collimated by a lens (35 mm). The acquisition was done using a monochrome CMOS camera (Thorlabs, CS2100M-USB), blinded to the LED light by a 550 nm long pass filter, that should provide transmittance of Eu^{2+} red emission. The camera was carefully aligned in respect to the chopper rotation axis to avoid tilt/shift artifacts in the image. Knowing the exact rotation speed of a chopper (estimated by a pulse-to-pulse time using an oscilloscope and a Si-photodiode), the time axis for lifetimes can be simply rebuilt using the number of pixels per decay time. Intensity decay profiles from acquired images were analyzed using the following Python script (see Supporting Information).

Supporting Information

Supporting Information is available from the Wiley Online Library or from the author.

Acknowledgements

The financial support provided by the Helmholtz Association is gratefully acknowledged: i) a Recruitment Initiative Fellowship for B.S.R.; ii) the funding of chemical synthesis equipment from the Helmholtz Materials Energy Foundry (HEMF); and iii) Research Field Energy – Program Materials and Technologies for the Energy Transition – Topic 1 Photovoltaics (38.01.05). B.S.R. and A.T. acknowledge funding from the European Union's Horizon 2020 research and innovation project "Circular Foodpack" agreement No: 101003806. The authors would like to acknowledge the help of Prof. Hendrik Swart (UFS, South Africa) in interpreting the TL results, and that of Yang Lu in performing the XRD analysis for the revised version of the manuscript.

Conflict of Interest

The authors declare no conflict of interest.

Author Contributions

A.C.E. conducted a thorough evaluation of synthetic protocols from the literature, developed modifications to the synthetic procedures, synthesized all samples, performed X-ray diffraction and scanning electron microscopy measurements, and proofread the document. E.M. led the photophysical characterization of all samples and demonstration experiment; D.B. contributed to the demonstration experiment and measurements of TL curves; I.A.H. contributed to the conception of manuscript and proofreading; B.S.R. secured financial support for the project (personnel and equipment), contributed to the conceptualization of the experiments and manuscript, and provided several founds of critical proofreading (regarding both structure and wording of the manuscript); A.T. contributed to the conception of the experiments and the manuscript, supervised the experiments, performed the stability test, wrote large parts of the text for the manuscript, proofread the document and handled the submission process.

Data Availability Statement

The data that support the findings of this study are available from the corresponding author upon reasonable request.

Keywords

persistent luminescence, photoluminescence quantum yield, plastic sorting, tracer based sorting

Received: February 20, 2025
Revised: May 23, 2025
Published online: June 22, 2025

[1] a) I. A. Howard, D. Busko, G. Gao, P. Wendler, E. Madirov, A. Turshatov, J. Moesslein, B. S. Richards, *Resour., Conserv. Recycl.* **2024**, *205*, 107557; b) J. Woidasky, I. Sander, A. Schau, J. Moesslein, P. Wendler, D. Wacker, G. Gao, D. Kirchenbauer, V. Kumar, D. Busko, I. A. Howard, B. S. Richards, A. Turshatov, S. Wiethoff, C. Lang-Koetz, *Resour., Conserv. Recycl.* **2020**, *161*, 104976; c) R. R. Larder, F. L. Hatton, *ACS Polymers Au* **2023**, *3*, 182.
[2] S. Brunner, P. Fomin, C. Kargel, *Waste Manage.* **2015**, *38*, 49.
[3] G. Gao, A. Turshatov, I. A. Howard, D. Busko, R. Joseph, D. Hudry, B. S. Richards, *Adv. Sustain. Syst.* **2017**, *1*, 1600033.
[4] K. Rajagopalan, E. Madirov, D. Busko, I. A. Howard, B. S. Richards, H. C. Swart, A. Turshatov, *ACS Appl. Mater. Interfaces* **2023**, *15*, 43985.
[5] a) H. Langhals, D. Zgela, T. Schlücker, *Green and Sustain. Chem.* **2014**, *4*, 144; b) A. Monteleone, F. Wenzel, H. Langhals, D. Dietrich, *J. Environ. Chem. Eng.* **2021**, *9*, 104769.
[6] Y. Lu, J. Lu, J. Zhao, J. Cusido, F. M. Raymo, J. Yuan, S. Yang, R. C. Leif, Y. Huo, J. A. Piper, J. Paul Robinson, E. M. Goldys, D. Jin, *Nat. Commun.* **2014**, *5*, 3741.

© 2025 The Author(s). Advanced Materials Technologies published by Wiley-VCH GmbH

2365709x, 2025, 19, Downloaded from https://advanced.onlinelibrary.wiley.com/doi/10.1002/admt.202500353 by Karlsruher Institut Für Technologie, Wiley Online Library on [19/11/2025]. See the Terms and Conditions (https://onlinelibrary.wiley.com/terms-and-conditions) on Wiley Online Library for rules of use; OA articles are governed by the applicable Creative Commons License

[7] A. Becker, K. Luttermann, U. Claussen, P. Orth, L. Heiliger, A. E. Sayed, Patent US5329127A **1993**.
[8] P. G. Harris, R. G. Fern, J. Silver, Patent GB2561597B **2017**.
[9] N. Katumo, L. A. Ruiz-Preciado, V. Kumar, G. Hernandez-Sosa, B. S. Richards, I. A. Howard, *Adv. Mater. Technol.* **2021**, *6*, 2100047.
[10] N. Katumo, K. Li, B. S. Richards, I. A. Howard, *Sci. Rep.* **2022**, *12*, 2100.
[11] a) P. F. Smet, I. Moreels, Z. Hens, D. Poelman, *Materials* **2010**, *3*, 2834; b) D. Kim, *Nanomaterials* **2021**, *11*, 723.
[12] J. Du, D. Poelman, *J. Phys. Chem. C* **2020**, *124*, 16586.
[13] S. Rekha, E. I. Anila, *Mater. Chem. Phys.* **2019**, *237*, 121843.
[14] a) D. C. Rodríguez Burbano, E. M. Rodríguez, P. Dorenbos, M. Bettinelli, J. A. Capobianco, *J. Mater. Chem. C* **2014**, *2*, 228; b) Y. Liang, J. He, Z. Song, Y. Han, Z. Qiu, W. Zhou, J. Zhang, L. Yu, S. Lian, *ACS Appl. Mater. Interfaces* **2022**, *14*, 1413.
[15] Y. Tamura, T. Okuno, Y. Suda, Y. Nanai, *J. Phys. D: Appl. Phys.* **2020**, *53*, 155101.
[16] X. Wang, Z. Qiu, Y. Li, Q. Mi, W. Zhou, S. Ai, J. Xu, Y. Liu, S. Lian, *J. Mater. Chem. C* **2019**, *7*, 5931.
[17] J. E. Van Haecke, P. F. Smet, K. De Keyser, D. Poelman, *J. Electrochem. Soc.* **2007**, *154*, J278.
[18] K. N. Kim, J.-M. Kim, K. J. Choi, J. K. Park, C. H. Kim, *J. Am. Ceram. Soc.* **2006**, *89*, 3413.
[19] a) Z. Qiu, C. Rong, W. Zhou, J. Zhang, C. Li, L. Yu, S. Liu, S. Lian, *J. Alloys Compd.* **2014**, *583*, 335; b) C. Guo, D. Huang, Q. Su, *Mater. Sci. Eng., B* **2006**, *130*, 189.
[20] *Chin. Phys. B* **2014**, *23*, 087808.
[21] H. S. Kim, T. Horikawa, H. Hanzawa, K.-i. Machida, *J. Phys.: Conf. Ser.* **2012**, *379*, 012016.
[22] D. N. Game, N. B. Ingale, S. K. Omanwar, *J. Mater. Sci.: Mater. Electron.* **2017**, *28*, 915.
[23] M. D. Mehare, C. M. Mehare, H. C. Swart, S. J. Dhoble, *Prog. Mater. Sci.* **2023**, *133*, 101067.
[24] C. Guo, B. Chu, M. Wu, Q. Su, Z. Huang, *Journal of Rare Earths* **2003**, *21*, 501.
[25] D. C. Rodríguez Burbano, S. K. Sharma, P. Dorenbos, B. Viana, J. A. Capobianco, *Adv. Opt. Mater.* **2015**, *3*, 551.
[26] E. Madirov, D. Busko, F. A. Cardona, D. Hudry, S. V. Kuznetsov, V. A. Konyushkin, A. N. Nakladov, A. A. Alexandrov, I. A. Howard, B. S. Richards, A. Turshatov, *Adv. Photonics Res.* **2023**, *4*, 2200187.
[27] Y. Liu, Y. Ding, Z. Peng, Q. Yu, X. Tian, G. Dong, *Ceram. Int.* **2014**, *40*, 5061.
[28] X. Zhang, J. Su, X. Yan, Y. Liao, Z.-c. Wu, C. Zhou, *Solid State Sci.* **2020**, *99*, 106050.
[29] H. A. A. Seed Ahmed, H. C. Swart, P. Bergman, R. E. Kroon, *Mater. Res. Bull.* **2016**, *75*, 47.
[30] V. Castaing, M. Romero, D. Rytz, G. Lozano, H. Míguez, *Adv. Opt. Mater.* **2024**, *12*, 2401638.
[31] G. Sivakumar, A. T. Muhammed Munthasir, P. Thilagar, S. Natarajan, *Chem. Mater.* **2024**, *36*, 5356.
[32] S. K. Gupta, K. Sudarshan, D. Chandrashekhar, A. Balhara, M. Mohapatra, *J. Lumin.* **2023**, *257*, 119697.
[33] S. G., D. Hebbar N, S. G. Menon, P. M. Lewis, K. S. Choudhari, R. E. Kroon, H. C. Swart, S. D. Kulkarni, *Optical Materials* **2022**, *123*, 111919.
[34] M. Li, H. Zhang, X. Zhang, J. Deng, Y. Liu, Z. Xia, B. Lei, *Mater. Res. Bull.* **2018**, *108*, 226.
[35] M. Koehl, S. Hoffmann, S. Wiesmeier, *Prog. Photovolt.* **2017**, *25*, 175.
[36] S. N. Jayaramu, E. Coetsee, J. Hölsä, H. C. Swart, *Phys. Scr.* **2024**, *99*, 115975.
[37] S. N. Jayaramu, D. Janardhana, L. J. B. Erasmus, E. Coetsee, D. E. Motaung, H. C. Swart, *Dalton Trans.* **2024**, *53*, 16557.

© 2025 The Author(s). Advanced Materials Technologies published by Wiley-VCH GmbH

2365709x, 2025, 19, Downloaded from https://advanced.onlinelibrary.wiley.com/doi/10.1002/admt.202500353 by Karlsruher Institut Für Technologie, Wiley Online Library on [19/11/2025]. See the Terms and Conditions (https://onlinelibrary.wiley.com/terms-and-conditions) on Wiley Online Library for rules of use; OA articles are governed by the applicable Creative Commons License